Space Sci Rev
DOI 10.1007/s11214-007-9259-2

The STEREO/IMPACT Magnetic Field Experiment

M.H. Acuña · D. Curtis · J.L. Scheifele · C.T. Russell · P. Schroeder · A. Szabo · J.G. Luhmann

Received: 20 March 2007 / Accepted: 7 August 2007

Abstract The magnetometer on the STEREO mission is one of the sensors in the IMPACT instrument suite. A single, triaxial, wide-range, low-power and noise fluxgate magnetometer of traditional design—and reduced volume configuration—has been implemented in each spacecraft. The sensors are mounted on the IMPACT telescoping booms at a distance of ∼3 m from the spacecraft body to reduce magnetic contamination. The electronics have been designed as an integral part of the IMPACT Data Processing Unit, sharing a common power converter and data/command interfaces. The instruments cover the range ±65,536 nT in two intervals controlled by the IDPU (±512 nT; ±65,536 nT). This very wide range allows operation of the instruments during all phases of the mission, including Earth flybys as well as during spacecraft test and integration in the geomagnetic field. The primary STEREO/IMPACT science objectives addressed by the magnetometer are the study of the interplanetary magnetic field (IMF), its response to solar activity, and its relationship to solar wind structure. The instruments were powered on and the booms deployed on November 1, 2006, seven days after the spacecraft were launched, and are operating nominally. A magnetic cleanliness program was implemented to minimize variable spacecraft fields and to ensure that the static spacecraft-generated magnetic field does not interfere with the measurements.

Keywords STEREO mission · IMPACT · Space weather · Interplanetary medium · Solar physics

PACS 96.50.Ry · 96.50.Qx · 96.50.sh · 96.50.Xy · 96.60.Ly · 96.60.-j

M.H. Acuña (✉) · J.L. Scheifele · A. Szabo
NASA Goddard Space Flight Center, Greenbelt, MD, USA
e-mail: mario.acuna@nasa.gov

D. Curtis · P. Schroeder · J.G. Luhmann
Space Sciences Laboratory, University of California, Berkeley, CA, USA

C.T. Russell
Institute of Geophysics and Planetary Physics, University of California, Los Angeles, CA, USA

1 Introduction

The STEREO IMPACT investigation incorporates a suite of instruments designed to address important elements of the primary science objectives of the mission (see Luhmann et al. 2007). The interplanetary magnetic field (IMF) structure and dynamics represent an extension of the solar magnetic field as carried out from the Sun by the supersonic solar wind. The IMPACT magnetometer experiment will continuously measure the time-variable, large-scale structure of the IMF at both locations of the STEREO spacecraft in their orbits and in particular the gradients between them indicative of small-scale structures possibly associated with transient events. These measurements will allow us to interpret solar wind parameters, particle distribution functions, the paths followed by energetic particles detected at the spacecraft. We will also be able to analyze local sources for in-situ acceleration mechanisms such as shocks and discontinuities. The experiment incorporates fast measurement capabilities that will allow the characterization of IMF fluctuations over a wide range of frequencies spanning multi-year solar cycle variations to proton gyrofrequencies; this allows the study of microscale phenomena in the solar wind. The magnetic field measurements provide a fundamental frame of reference for defining the background on which multiple interplanetary physics phenomena take place. Of particular interest to the twin spacecraft STEREO mission are those associated with solar transient events that affect the Earth's immediate environment.

The magnetometer provides continuous measurements of the local IMF at both spacecraft locations, with an intrinsic sample rate of 32 samples/s. Raw data at this sampling rate are delivered to the IMPACT suite Digital Processing Unit (IDPU) for processing, packetization and transmission to the ground as well as for use by other IMPACT experiments onboard. The measurements are precise (16-bit A/D converter or 0.003% of full scale) and sensitive (0.015 nT), with an absolute accuracy goal of $\sim$0.1 nT. The intrinsic noise level of the magnetometer has the typical $1/f$ spectrum associated with fluxgate sensors (Acuña 2002) and references therein) with a baseline value of 10^{-5} nT^2/Hz at 1 Hz. At $\sim$10 Hz the spectrum flattens out to a value of $\sim 10^{-6}$ nT^2/Hz. The integrated RMS noise in the 0.001–1 Hz frequency range is typically $<$0.01 nT so instrument noise, and its effect on the measurements, is minimal.

The instrument configuration aboard each spacecraft consists of a single triaxial sensor mounted approximately two-thirds of the way along a four-meter deployable boom, or three meters from the edge of the spacecraft bus. This boom is shared with other IMPACT suite instruments, as illustrated in Figs. 1a and 1b. The sensor location represents a reasonable compromise among many conflicting requirements. The telescoping boom (Luhmann et al. 2007) includes a 25-cm tray attached perpendicular to the boom axis on which the magnetometer sensor is mounted. This tray is necessary to place the sensor away from possible interference from magnetic fields created by the signals and currents flowing in the boom harness that supplies power and signals to other experiments on the boom. The triaxial sensor assembly is shown in Fig. 2 and measures $10.8 \times 6.4 \times 6.4$ cm. Boom deployment for both spacecraft took place on November 1, 2006, seven days after launch while the spacecraft were in a low magnetic field environment. Both magnetometer instruments have remained on since their activation on that date. The signal processing portion of the magnetometer electronics was implemented within the IMPACT instrument data processing unit (IDPU), on a $19.6 \times 15.6 \times 2.0$ cm frame that supports the main board and three 16-bit sigma-delta analog to digital converters. The complete assembly is shown in Fig. 3. A common power converter is shared between the IDPU and magnetometer electronics, whose power consumption is $\sim$0.5 watts (not including heater power). The thermal environment

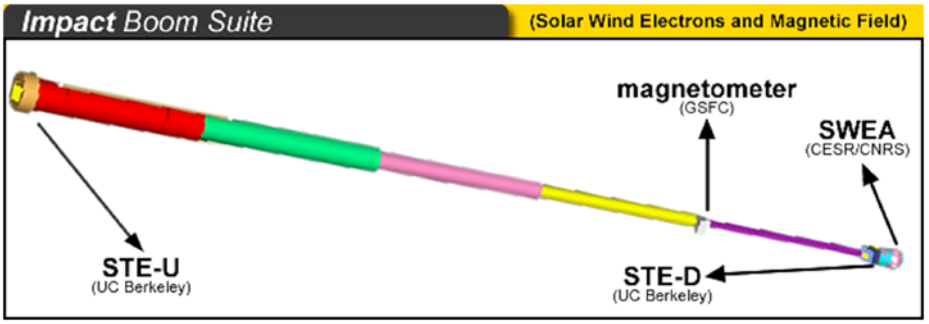

(**a**)

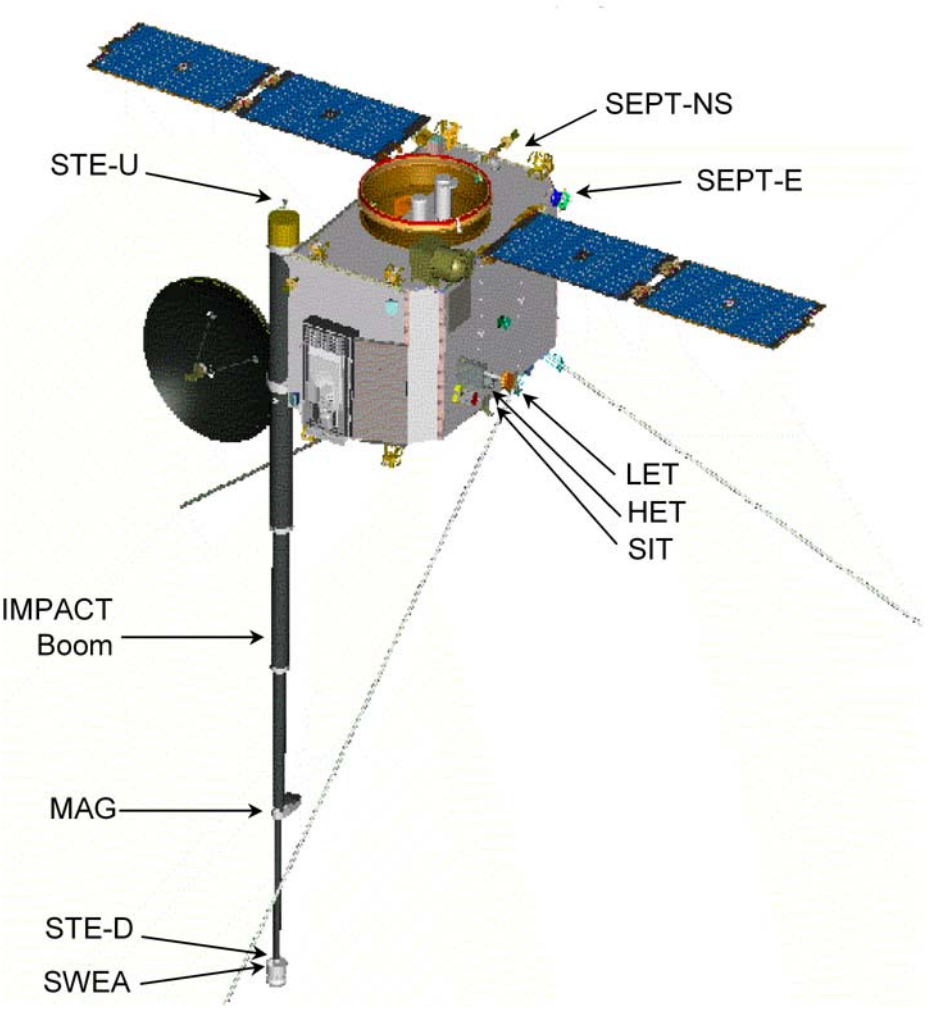

(**b**)

Fig. 1 (**a**) The STEREO deployable boom and the location of IMPACT suite sensors. The MAG sensor is approximately 1.5 m inboard from the SWEA/STE-D sensors. (**b**) Relative placement of the IMPACT boom on the STEREO spacecraft. Other IMPACT suite sensors are also shown for reference

Fig. 2 The triaxial MAG sensor assembly, cover and baseplate. The sensor is thermally isolated from the mounting surface by four acetal legs. A foil heater used to adjust the assembly temperature is also visible on the underside of the sensor base. In the final configuration the sensor is wrapped with a 20-layer, grounded thermal blanket that also acts as an electrostatic shield

Fig. 3 The IMPACT/MAG electronics assembly. This "slice" or frame is incorporated within the IDPU assembly that provides interfaces and power. It weighs 232 grams and requires 0.48 watts of power. A combination of surface mount and through-hole components are used to meet stringent performance and quality requirements

of the magnetometer sensor assembly is controlled by the use of thermal blankets and a thermofoil heater that supplies up to 1.2 watts of power at 50 kHz, controlled by a dedicated pulse-width-modulation (PWM) circuit. This AC power system is required to avoid the introduction of stray magnetic fields that a DC heater can generate and its operating frequency is crystal controlled to avoid interference with the SWAVEs experiment onboard.

The performance of the IMPACT/magnetometer sensors is typical of that of low-noise, ring-core magnetometers that have been widely used in space missions (Acuña 2002). The zero levels including spacecraft contributions are estimated by means of periodic roll maneuvers about the Earth-pointed spacecraft axis and use of the statistical properties of the interplanetary magnetic field (Schwarzl and Russell 2007). Maneuvers about a second axis, perpendicular to the roll axis, are not allowed by spacecraft safety constraints. As mentioned earlier the instrument incorporates two dynamic ranges (low and high) that can be switched by automatic or manual control. Since the low range upper limit is 512 nT, frequent range changes are not expected when the spacecraft are in their final orbits in the solar wind. However, this wide-range measurement capability is extremely useful during the early part of the

mission when the "phasing" orbits required to inject the spacecraft into their final orbits place them in regions of strong fields.

2 Science Objectives

The overall science objectives of the STEREO mission are: understanding the causes and mechanisms of Coronal Mass Ejection (CME) initiation; characterizing the propagation and evolution of CMEs through the heliosphere; discovering the mechanisms and sites of energetic particle acceleration in the low corona and interplanetary medium; and developing a 3-D time-dependent model of the magnetic topology, temperature, density and velocity structure of the ambient solar wind. The IMPACT investigation addresses these objectives through synergistic measurements of plasma parameters, energetic charged particles and in-situ magnetic fields. The IMPACT fluxgate magnetometer makes significant contributions to all of these objectives.

2.1 CME Identification and Structure

Various parameters are used to identify the boundaries of the interplanetary manifestation of CMEs (ICMEs) often yielding significantly different results for the same event (Zwickl et al. 1983; Neugebauer and Goldstein 1997; Mulligan et al. 1999; and Burlaga et al. 2001). Easiest to identify are magnetic clouds that have slowly rotating strong magnetic fields with a suppressed level of field fluctuations (e.g., Burlaga 1995). In-situ vector magnetic field observations have been used with great success to model these structures as force-free magnetic flux ropes (e.g., Lepping et al. 2006 and references within; also see Fig. 4). Burlaga et al. (1990) used measurements from four spacecraft—Helios I and II, IMP 8 and Voyager (see Fig. 5)—to determine the global shape or geometry of the magnetic clouds. Mulligan et al. (1999) and Mulligan and Russel (2001) used data from the WIND, NEAR and ACE spacecraft to study CME's and associated IMF structures for selected events. With the two STEREO spacecraft and near Earth observations, this will be routinely accomplished. Current MHD models simulating the evolution of magnetic clouds in the heliosphere predict significant deviation from cylindrical symmetry by 1 AU (e.g., Odstrcil et al. 2004) or even indentations at streamer belt latitudes as the faster moving high-latitude portions of the cloud leave the low-latitude segments behind (Kasper and Manchester 2007). With fortuitous orientation of magnetic clouds, STEREO multi-point magnetic field and plasma observations will be able to determine the validity of these predictions.

The internal structure of magnetic clouds is often very complex. Counterstreaming halo electron measurements have demonstrated that often both foot points of a flux rope are still connected to the Sun when the cloud passes 1 AU (Gosling 1990). However, WIND observations revealed intermittent time periods when some internal field lines disconnected at one or both foot points from the Sun (Larson et al. 1997). Since most magnetic clouds will not pass exactly half way in between the two STEREO spacecraft, thus providing ICME cross-sections at different times, the IMPACT observations will give a glimpse into the time evolution of the internal field line structure of magnetic clouds by comparing the time periods of solar disconnections.

Magnetic clouds represent only 30% to 50% of the total ICMEs observed at 1 AU (Gosling 1990) with possible solar cycle dependence (Richardson and Cane 2004). The physical reasons for the existence of these complex ejecta is not established at this time, but they are due to either interaction between colliding ICMEs or they reflect

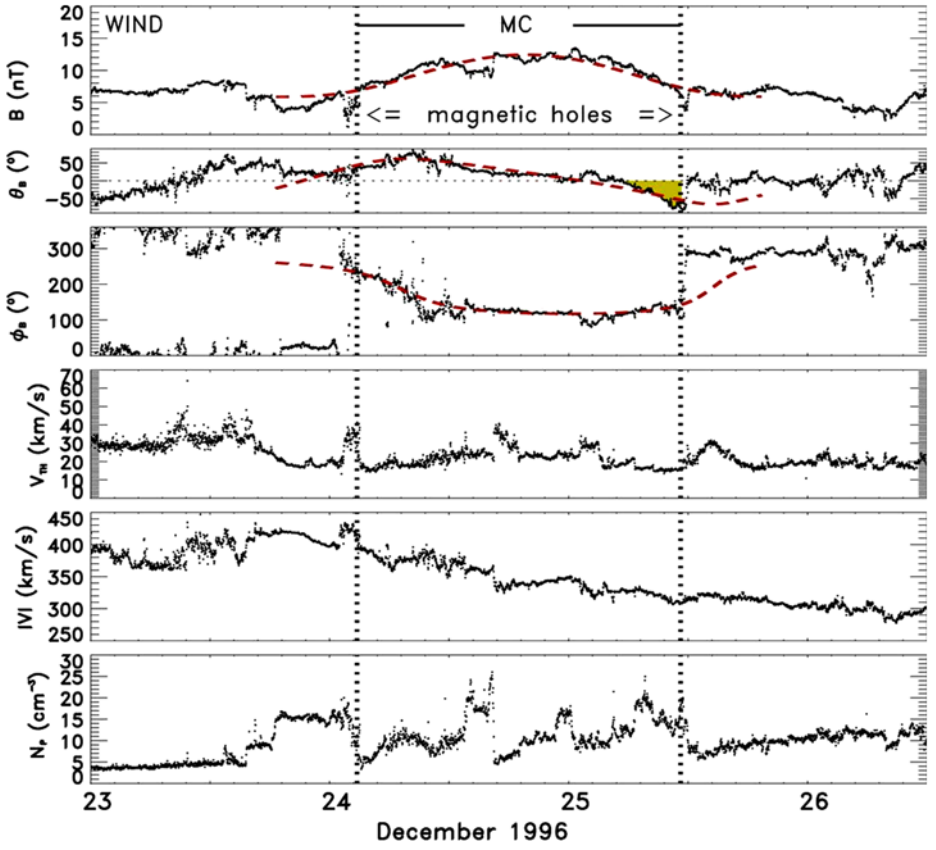

Fig. 4 A magnetic cloud observed by WIND on December 24–25, 1996. The panels are, *top to bottom*, magnetic field strength, elevation and azimuth angle of the magnetic field direction, solar wind proton thermal speed, proton speed and density. The *dotted vertical lines* indicate the magnetic cloud boundaries identified based on field signatures. The *dashed curves* are the result of a constant alpha force-free flux rope fit to the observations (based on Lepping et al. 2006)

a more dynamic coronal magnetic structure during their initiation (Burlaga et al. 2001; Richardson and Cane 2004); or the magnetic cloud forms only part of the ICME structure and is not penetrated on most encounters. In either case, in situ observations of the internal fields and plasma properties at longitudinally widely separated locations of the same complex ICME will provide hints concerning their genesis.

2.2 CME-Driven Interplanetary Shocks

Coronagraph and radio observations show that fast ICMEs often drive interplanetary shocks in front of them. Moreover, statistical studies have established that these interplanetary shocks tend to be the strongest in front of the nose of the driving ICME (Cane 1988; Richardson and Cane 1993). However, it has not been determined how much wider the longitudinal extent of the driven shock is and indeed whether all interplanetary shocks observed at 1 AU are due to fast ICMEs. Observing the same shock at significantly different longitudinal positions will provide this information. High time resolution magnetic field

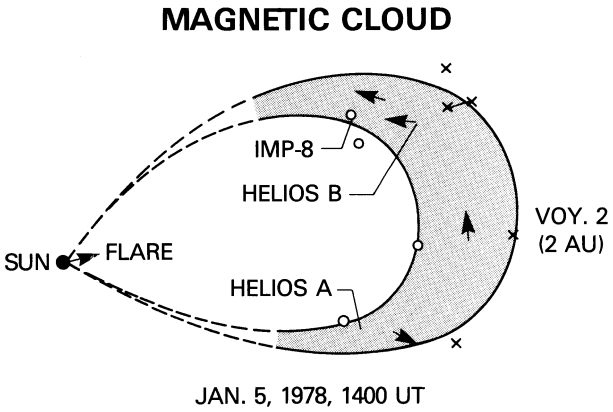

Fig. 5 The global shape of a magnetic cloud deduced from the four spacecraft observation of the January 5, 1978 event. Helios 1 and 2, IMP 8 and Voyager 2 measurements were used by Burlaga et al. (1990)

observations provided by the magnetometer will be essential to identify the shocks and to differentiate them from more gradually increasing pressure pulses.

The ICMEs do not propagate into a uniform interplanetary medium. Hence the driven shock surfaces are not expected to have a simple slowly changing curved geometry. In fact, near-Earth multi-spacecraft analysis of the same interplanetary shocks have found significant deviation from planarity (Russell et al. 1983; Szabo et al. 2001; Szabo 2005) indicating ripples on the shock surface with a ∼100 Earth radii scale length. Specifically, Szabo et al. (2001) found—analyzing a few ACE, WIND and IMP 8 observed interplanetary shocks—that with larger inter-spacecraft separation, perpendicular to the solar wind flow direction, larger angular deviation between individually determined shock normals was likely. Supporting this result, WIND electron observations reveal cases where backstreaming electrons at nearly perpendicular shocks imply local shock surface bays of similar scale (Bale et al. 1999). The two STEREO spacecraft will provide much larger longitudinal separations than past near-Earth spacecraft, allowing the full characterization of both local and global geometry of interplanetary shock surfaces.

Interplanetary shocks are not simple step functions in solar wind parameters but have complex, non-MHD or kinetic internal structure composed of the shock foot. The shock foot is characterized by a small but systematic increase in the magnetic field over the steady solar wind values, immediately upstream. It is generally attributed to the presence of reflected ions from the shock (e.g., Paschmann et al. 1982). After the foot, the magnetic field increases sharply in the ramp, reaching values well above the steady downstream conditions thus producing the overshoot. After the peak of the overshoot, a strongly damped oscillation occurs until conditions stabilize on the downstream side. The thicknesses of the various microstructure features and the size and gradient of the ramp have strong impact on the ability of shocks to accelerate particles. The detailed mechanism behind this is still not clear. The STEREO magnetometer will provide the necessary high time resolution (∼100 ms) magnetic field observations to resolve the various internal shock structures allowing the correlation of locally observed energetic particle characteristics to shock microstructure details.

2.3 Acceleration of Particles at Interplanetary Shocks

Interplanetary shocks are very effective in accelerating charged particles to very high energies. Thus, a large fraction of Solar Energetic Particles (SEPs) are thought to be generated by shocks driven by fast-moving CMEs. The seed particles are energized as

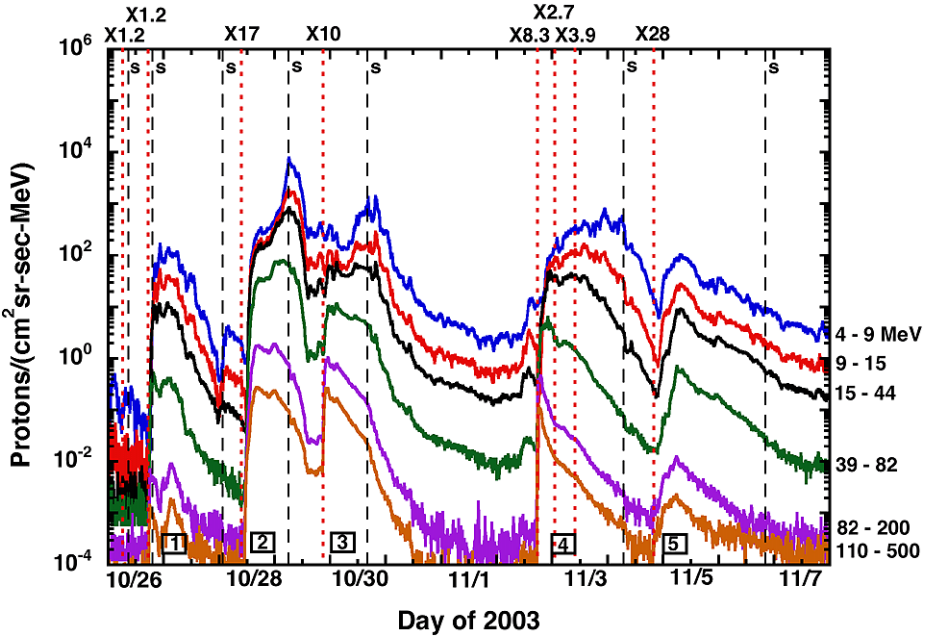

Fig. 6 Proton data measured by GOES-11 in six different energy intervals during the October–November 2003 events. *Vertical dashed lines* indicate the occurrence of X-class flares and the *dotted lines*, marked by an "*s*", label the passage of interplanetary shocks at 1 AU. Note the additional particle enhancements at the time of shock crossings (after Mewaldt et al. 2005)

they cross back and forth the shock numerous times. This process of diffusive or first-order Fermi acceleration leads to a power-law spectrum of the accelerated particles that is typically observed in interplanetary space (e.g., Zank et al. 2005). The detailed characteristics of the shock, such as the shock strength and the angle between the shock normal and the upstream magnetic field, determine the effectiveness of the acceleration process. Though the highest energy particles are generated very close to the Sun, interplanetary shocks at 1 AU still accelerate particles allowing an insight into the details of the energization process (see Fig. 6). The magnetometer will provide the necessary high time resolution vector measurements of the local magnetic field that is required as input for current state-of-the-art shock-fitting methods (e.g., Viñas and Scudder 1985; Szabo 1994) yielding shock speeds, normal directions and detailed characteristics required to compare theoretical predictions to in-situ observations.

For diffusive shock acceleration to work, a certain degree of magnetic field turbulence upstream and downstream of the shock is necessary to scatter the particles. In turn, the accelerated particles themselves generate turbulence resulting in a complex relationship between the shock properties, the acceleration mechanism and turbulence wave intensity (e.g., Lee 1983; Gordon et al. 1999; Li et al. 2005). In situ particle spectra and magnetic field fluctuation levels observed by ISEE 3 (Sanderson et al. 1985) and more recently by SOHO and ACE (Bamert et al. 2004) have shown correlation between the energetic particle intensity and the wave power density near the shock front. However, these studies were limited to a single point along the shock surface. The STEREO mission, in conjunction with near Earth spacecraft, allows the observation of particle intensities and magnetic turbulence levels at three points with increasing separation, thus allowing the separation of local and global processes.

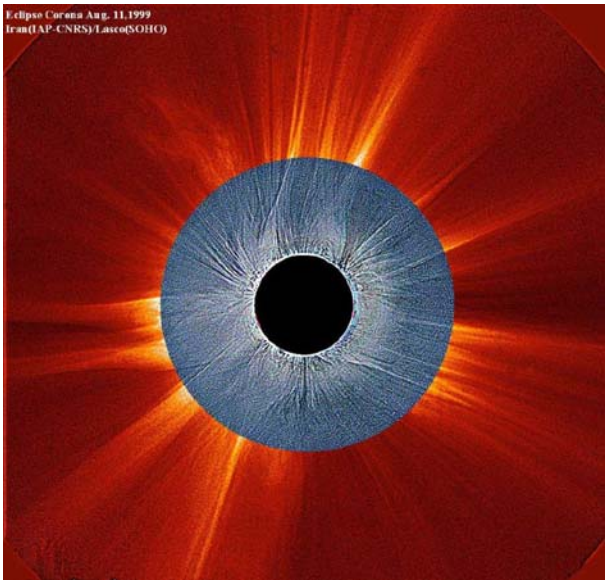

Fig. 7 Composite image of the corona at the time of the eclipse on August 11, 1999 (Koutchmy et al. 2004). The fine-scale structure of the corona is clearly visible in the inner heliosphere, though it might be completely washed out by 1 AU

The STEREO magnetometer will provide high time resolution magnetic field observations that can be used to compute the required power spectral densities to above 10 Hz. This rate is sufficient to resolve ion kinetic phenomena at an interplanetary traveling shock.

2.4 Global Structure of the IMF

An important scientific objective of the STEREO mission is to determine the ambient solar wind structure. The two spacecraft will provide a lengthening baseline for measuring the geometry of interplanetary wave fronts and discontinuities—including the heliospheric current sheet (e.g., Szabo et al. 1999)—on multiple spatial scales. This type of study has been performed using, for example, IMP 8 and WIND observations (Richardson and Paularena 1998) on a limited, near-Earth scale. The STEREO observations will greatly extend the range of the transverse scales accessible.

The spectrum of the magnetic and to some extent other solar wind fluctuations as a function of wave vector is required for understanding the heliospheric turbulent cascade and thus the heating due to these processes; for determining the interaction of the fluctuations with energetic particles and thus the modulation of cosmic ray fluxes; and, by extrapolation back to the Sun, for elucidating the wave-generation mechanisms (e.g., Roberts et al., 1987, 1992). By making measurements at varying spatial scales (different frequency bands in the time series analysis) and at different spacecraft separations, the time scale of persistent features on the Sun that lead to interplanetary disturbances can be determined. It is known that stream structure is due to persistent features, but it is unclear the extent to which "microstreams"—narrow streams within larger streams—are of solar origin (as suggested by modern high-resolution coronagraph images such as Fig. 7) or are generated in transit. STEREO observations will provide the opportunity to resolve this issue.

2.5 Space Weather

The STEREO real-time telemetry capability will enable a number of different space weather forecasting techniques based on CME and flare remote sensing or field line tracing with

energetic particles. Moreover, the slowly increasing longitudinal separation between the two STEREO spacecraft will allow the determination of the typical angular width of ICMEs and high-energy particle beams. Real-time in situ magnetic field data will be essential for the forecasting of geomagnetic events caused by high-speed streams. As the Sun spins, the spacecraft lagging behind Earth will encounter the compressed fields at the leading edge of high speed streams many hours to days in advance of where they impinge on the Earth's magnetosphere causing sudden commencements and possibly geomagnetic storms (StCyr and Davila 2001). Since recurring high-speed streams have a relatively simple and well-known structure, the low cadence real time telemetry mode of STEREO will be sufficient for this purpose.

3 IMPACT/MAGNETOMETER Performance Requirements

The magnetometer performance capabilities were optimized to address the scientific objectives and to make synergistic use of limited spacecraft resources. To support measurements over the range of expected fields, both in the final and phasing orbits as well as during test and integration in Earth's field, the instruments provide a low or fine range covering ± 512 nT for each of three orthogonal axes and a high or coarse range covering $\pm 65{,}536$ nT. The desired absolute accuracy in the low range to meet the science objectives is ~ 0.1 nT and this goal requires that the spacecraft magnetic field at the magnetometer sensor vary by less than ~ 0.03 nT and that the sensor orientation be known to $\pm 0.5^\circ$ with respect to inertial coordinates. To achieve the magnetic cleanliness goals, a Magnetics Control Plan was implemented; this is described in more detail in Sect. 6 The onboard magnetic measurements must be digitized to a resolution of 16-bits internally for digital processing to provide a resolution of 2.0 nT in the high or coarse range and 0.015 nT resolution in the low or fine range. The scale factors and alignments must be known such that an overall accuracy better than $\sim 1\%$ of the ambient field and ~ 1 degree in alignment is achieved. These values need to be determined in a high field environment such as the Earth's field and extrapolated by laboratory measurements to the low field levels of the IMF (Merayo et al. 2000).

Table 1 shows a summary of the goals and relevant technical performance parameters required for the IMPACT/magnetometer. The availability of flight-qualified, high-resolution sigma-delta analog-to-digital converters allowed the simplification of the multi-range designs used in earlier missions to the one described for STEREO using only two dynamic ranges without loss of performance. Automatic range switching is a requirement and must be controlled automatically by commands from the IDPU in response to the intensity of the ambient field or manually commanded from the ground. The need for increased sampling

Table 1 IMPACT MAG performance characteristics

Description	Goal	Requirement
Noise level	0.01 nT	0.05 nT
Absolute accuracy	± 0.1 nT	± 0.1 nT
Range	± 512 nT, $\pm 65{,}536$ nT	± 512 nT
Drift	± 0.2 nT/yr	± 0.2 nT/yr
Time resolution	1/8 s (Normal) 1/32 s (Burst) 10 s (Beacon)	1 s

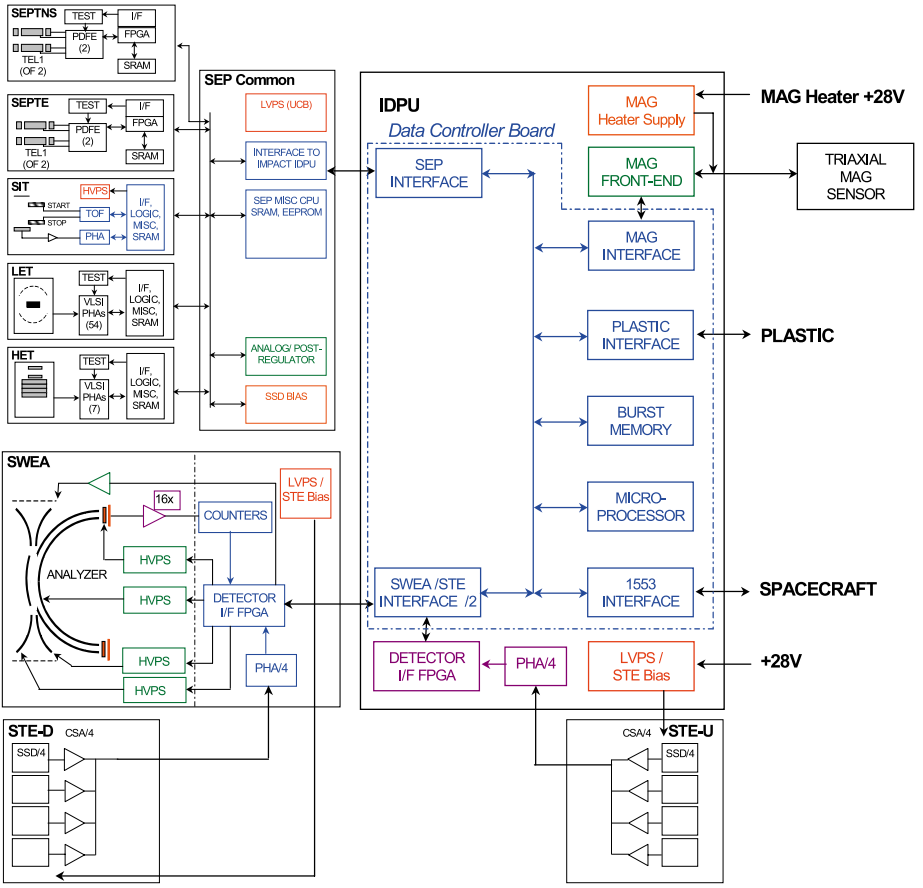

Fig. 8 Block diagram of the IMPACT instrument suite and IDPU illustrating the components associated with the MAG signal and data processing electronics. A separate MAG sensor heater PWM controller operating at a crystal controlled frequency of 50 kHz is also shown

rates in high time resolution modes required that the magnetic data be sampled internally at a constant rate of 32 samples/s. The IDPU must process these "raw" data in one of several formats to deliver the final data structure to the spacecraft packetized telemetry system and for distribution to other users. The IDPU as implemented for STEREO contains two general-purpose processors, a 1553 spacecraft interface, memory, and the necessary interface logic to connect to the magnetometer system. For reference, Fig. 8 shows a block diagram of the IDPU. This architecture defined the requirements for the magnetometer electronics interfaces. Mounting the sensor on a boom, coupled with a cost-effective, end-to-end spacecraft magnetic cleanliness program provides excellent overall performance and was the baseline chosen to satisfy all STEREO magnetic field measurement objectives. To achieve the desired measurement accuracy, STEREO required that a magnetic cleanliness program be implemented. The requirements formulated for the STEREO program included associated laboratory test instrumentation, training sessions and easy access by spacecraft subsystems builders and scientific experimenters to test and consulting resources. This approach has been pioneered by several space magnetic field measurements groups in the U.S.,

Europe and Japan and have been applied successfully to numerous space missions in the past (WIND/POLAR, Galileo, Cassini, Ulysses, CLUSTER II, Giotto, Geotail, ACE, MGS, LP, etc.). The IMPACT/magnetometer inflight instrument performance requirements include a self-calibration capability that can inject a known step-bias current in the sensor, corresponding to a magnetic field offset of approximately one-quarter of full scale along each axis. The IDPU is required to control this self-calibration function by means of commands programmed from the ground. The IMPACT/magnetometer instrument test and calibration requirements included laboratory calibrations and verification at the Goddard Space Flight Center and/or Wallops Island Magnetic Test Facilities, and finally at the system level after spacecraft integration. At this level two basic tests are required: (a) A "static" test to verify that the DC magnetic field generated by the spacecraft (unpowered) is below the required level (typically 1–3 nT), and (b) a "dynamic" test to verify that time-variable fields generated by spacecraft currents, motors, relays, etc. are below the ∼0.03 nT goal. The system level magnetic compatibility test requirements validate the effectiveness of the magnetics control plan implemented during the design, manufacturing and integration of the spacecraft subsystems. Finally, the magnetometer sensor requires that its temperature remain within an acceptable range and this must be achieved by an active temperature-control system. The heating element is typically a thermofoil heater attached to the magnetometer sensor assembly itself. DC current cannot be used to power this heater since small deviations from its non-inductive design introduce undesirable magnetic fields. A crystal-controlled pulse-width-modulator control circuit running at 50 kHz was chosen to provide AC power to the heater and maintain the sensor temperature in the range of $-25^\circ < T < 65^\circ$C.

4 Hardware Description

The STEREO IMPACT/magnetometer is a conventional three-axis fluxgate magnetometer design with extensive flight heritage derived from more than 50 space missions (Acuña 1974; Behannon et al. 1977; Potemra et al. 1985; Neubauer et al. 1987; Zanetti et al. 1994; Lohr et al. 1997; Acuña et al. 1992, 1997; Acuña 2002), implemented through a collaboration of NASA's Goddard Space Flight Center and the Space Sciences Laboratory of the University of California Berkeley. It also benefits significantly from the relevant experience gained through previous collaborations including Firewheel, Giotto, WIND, Mars Global Surveyor and Lunar Prospector. In the case of STEREO the conventional magnetometer design was updated with contemporary elements such as high-resolution sigma-delta analog-to-digital converters, surface mount devices and advanced microelectronics to minimize mass, volume and power resources. As mentioned previously, the basic instrument consists of an electronics board and frame mounted within the IMPACT IDPU enclosure and a triaxial sensor assembly mounted on the deployable IMPACT boom. These were illustrated in Figs. 2 and 3. The sensor assembly uses three orthogonally mounted ring core fluxgate sensors to derive vector components of the ambient field along the three directions. Small mechanical deviations from true orthogonality are corrected in ground processing using an "alignment matrix" determined in preflight calibration.

4.1 Analog Electronics

Figure 9 shows schematically a one-axis block diagram of the magnetometer analog signal processing electronics. The triaxial ring-core sensors are driven at 15.625 kHz (f_0) by a high-efficiency, nonlinear energy storage circuit that ensures that the cores are saturated

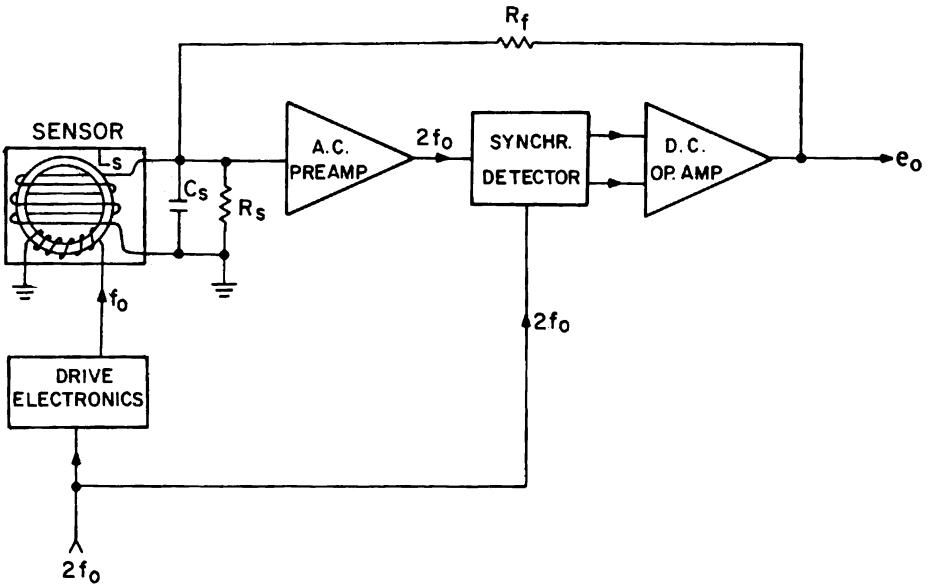

Fig. 9 Schematic block diagram of a one-axis fluxgate magnetometer. A ring core sensor is driven to saturation at frequency f_0 and the resulting signal at $2f_0$ (when a magnetic field is present) processed by the AC preamplifier, phase detector and DC amplifier (integrator) to generate a feedback current (e_0/R_f) that through the sense winding cancels the magnetic field sensed by the core

to more than 100 times their coercive force each cycle, eliminating memory effects (Acuña 1974). This drive signal is derived from a 125 kHz clock provided by the IDPU to control the analog-to-digital converters and interface logic. A related signal at twice the magnetometer excitation frequency (31.25 kHz) is also used as a reference to synchronously detect the amplified signals from the fluxgate sensors. In the absence of a magnetic field, the ring core sensors are balanced and no signal appears at the input of the AC preamplifier. When an external field is applied the sensor balance is disturbed and a signal containing only even harmonics of the excitation frequency appears at the input of the AC amplifier and is applied to the synchronous detector. The output from the synchronous detector is applied to a high gain DC integrator whose output voltage, through the resistor Rf, supplies enough current to null the field seen by the sensor and thus complete the feedback loop. The output voltage of the integrator is directly proportional to the magnitude and direction of the field with respect to each sensor axis orientation so three ring cores mounted orthogonal to each other provide full vector measurement capability. As mentioned earlier the intrinsic noise of the fluxgate sensors is $<$0.01 nT RMS (0.001–1 Hz). This level of noise is orders of magnitude smaller than that associated with IMF fluctuations and is adequate to detect all magnetic phenomena of interest to STEREO. Dynamic range changes are implemented by changing the parameters (by command) of the feedback resistor and the open loop gain of the AC input preamplifier while maintaining overall feedback loop stability. As already mentioned, the instrument has two dynamic ranges providing full-scale capabilities of $\pm$512 nT and $\pm$65,536 nT per axis. All three axes operate in the same range and range changes are synchronized with telemetry packet timing boundaries to allow unambiguous identification of range change events. The scale factor self-calibration function for the magnetometer is im-

plemented by introducing an offset step function into the voltage-to-current converter under IDPU control. The sensor heater AC controller is powered independently from the rest of the magnetometer electronics to allow temperature control when the IDPU is powered off. This high efficiency (>90%) controller includes a foldback current limiter that protects the spacecraft against catastrophic faults in the heater. The sensor assembly and foil heater are covered by a 20-layer thermal blanket to reduce radiative losses to a minimum. The maximum power that the heater controller can deliver is limited by design to <1.2 W.

4.2 Sigma-Delta A/D Conversion

The analog outputs of the magnetometer corresponding to the three orthogonal axes are sampled simultaneously with three independent 16-bit sigma-delta analog-to-digital (A/D) converters (Cirrus Logic CS5507) at a rate of 32 conversions per second. Monotonic time sampling is ensured by the use of a hardware-derived clock synchronized to the IDPU timing functions. A single-pole 16 Hz anti-alias low-pass filter is used on each channel to limit the input bandwidth to the A/D converters. The latter introduce additional poles at 20 Hz and above due to the decimation filters intrinsic to the converters. Detailed measurements of the magnetometer time response characteristics were acquired by activating the magnetometer calibration step function under IDPU control and monitoring the digital response. A self-calibration feature is integral to typical sigma-delta A/D converter features and updates the conversion scale factor and zero offset against a precision voltage reference. The IDPU initializes the A/D converters upon turn-on and can invoke the self-calibration feature by ground command. Periodic in-flight A/D calibrations are planned to correct any long-term drifts associated with the converter scale factors and offsets. The three A/D converters are triggered simultaneously every 31.25 ms to ensure simultaneous sampling and the resulting digital data are serially shifted into the IDPU under the logic control described below.

4.3 Control Logic and Interface to the IDPU

All logic, interface and command functions associated with the magnetometer electronics are implemented within a small gate-count, radiation-hard FPGA (Actel 1020). The automatic range-change algorithm implemented within the IDPU examines the digital values associated with each axis and if they exceed a predetermined threshold the instrument is commanded to the high range. Conversely, if the digital values are below a lower threshold the instrument is commanded to the low range. Manual commands can override the automatic function at any time. Range changes can take place only at defined packet time boundaries to eliminate ambiguities when the data are highly variable. The digitized data corresponding to the three magnetometer axes are shifted serially to the IDPU and stored in memory for further processing. Correspondingly, magnetometer commands, including calibration sequences, are delivered by the spacecraft to the IDPU, processed and shifted serially into the magnetometer control logic for execution.

5 IDPU Magnetometer Software

The IDPU magnetometer software manages data and command interface between the IDPU and magnetometer, performs several data-processing tasks and controls instrument operation. The command and interface functions include reception of commands from the spacecraft and implementation of these actions in the instrument. Data processing functions include reception of digital data from the magnetometer, time tagging, averaging, decimation

and formatting. The software also handles transmission of the instrument status, including housekeeping and safety data. The telemetry data structure consists of three formats and associated time series. The highest time resolution or "burst" data are made up of the high rate samples (32/s) without further processing. Burst data are collected continuously but only the "best data" are sent based on an onboard burst selection criteria extracted from the IMPACT instrument suite (see Luhmann et al. 2007). About 10 minutes of selected burst data are sent to the ground every three hours. The "normal" or continuous MAG data stream is generated by averaging the raw magnetometer data of 32 samples/s over four samples to generate 8 samples/s. A third format is associated with real time data sent to the ground continuously to monitor solar activity. This "beacon" format is a low rate, real time data stream consisting of 10-second averages of the ambient field. Magnetometer data are also used onboard for sorting SWEA electron data into pitch angle distributions. The data are averaged over two seconds (corresponding to the SWEA data collection time). Magnetometer offsets uploaded from the ground are subtracted and the field direction angles (azimuth and elevation) are computed in SWEA coordinates.

5.1 Range Control Strategy

The instrument range can be controlled in automatic or manual mode. In manual mode, the instrument range is set by command. In automatic range mode, the software compares the largest absolute value of the signed count values against the current range's full scale and adjusts the range if needed to maximize resolution while keeping the readings on scale. On startup, the range is controlled in automatic mode and the default range is low (± 512 nT full scale). The range control strategy must take into account the possibility of indefinite toggling between the two ranges for certain values of the field. To reduce this problem a hysteresis or "guard band" of digital values is used to avoid extended periods of saturation or conversely, low digital resolution data. All decisions associated with the range control function are based on the 32 samples/s data.

5.2 Internal Calibration

As described earlier, the magnetometer includes provisions for two types of internal calibrations that are exercised by ground command. The first is an analog magnetometer scale factor calibration capability that is implemented by injecting a known current into each of the fluxgate sensors equivalent to an external magnetic field of $1/4$ full scale amplitude. This function is controlled on and off by setting a control bit in the FPGA logic by ground command. Typically a series of commands are sent to turn the calibration step generator on and off and the resulting step amplitudes in the outputs are analyzed to monitor any scale factor variations. The second calibration function is associated with the capability of sigma-delta A/D converters to self-calibrate scale factors and offset. This function is invoked by setting the proper control bits "high" in the control register and it lasts two conversion cycles ($\sim$62 ms) during which time the A/D outputs no data (see CS5507 data sheet for additional details). The A/D self-calibration function is turned off automatically after the cycle is complete. During initial turn on the IDPU initializes the A/D by commanding a self-calibration to be executed. Further A/D calibrations can be invoked by ground command only to avoid affecting primary data during periods of high scientific interest.

6 Preflight Calibration and Testing

6.1 Scale Factors, Offsets and Alignment

The magnetometer electronics were initially adjusted for zero offset and approximate scale factor using a multilayer magnetic shield and calibration solenoids in the laboratory. These adjustments are generally sufficient to define these parameters to within ∼2% of their final values. Absolute scale factor calibration and relative sensor alignment measurements were conducted at the Goddard Space Flight Center and its Magnetics Test Facility. The absolute scale factor and relative alignment tests were derived using a modified version of the multiposition calibration technique described by Merayo et al. (2000). This technique yields extremely accurate values of alignment and scale factors but its application is restricted to the high range. The derived scale factors in this range were then transferred to a laboratory setup where the ambient magnetic field noise is minimal and small fields can be applied using a calibration solenoid. The zero field offsets were estimated by sensor rotations inside a magnetic shield where the residual field was less than 0.5 nT.

The scale factor and relative axis alignment technique consists of rotating the triaxial sensor assembly through 24 or more angular positions in a constant background field that is measured by means of a proton precession magnetometer. The measured field components (in digital counts or voltages) corresponding to each position and vector measurement are recorded and fitted to the model described later to minimize the residual error between the ambient and calculated total field. Precise angular positioning of the sensor is not required with this technique. However, the resulting alignment determination is relative to an arbitrarily chosen reference magnetic axis and not to a mechanical reference axis. Normally, the Earth's field can be used to establish the scale factor and relative alignment quickly and with acceptably small errors. This approach was used for the magnetometer calibration, and the ambient field used was that present at the 12 m GSFC magnetics test facility. If a reliable magnetics test facility is available, the procedure can be repeated for the low range to establish linearity. However, ambient magnetic noise limits the accuracy achievable. If we assume that the magnetometer linearity is of the order of 10^{-4} and the ambient field magnitude is constant for all sensor positions one can pose a linear least squares minimization problem to estimate the desired parameters (Merayo et al. 2000). Denoting the readings (counts) in the X, Y and Z axes by c_x, c_y and c_z and the fixed offsets as c_{x0}, c_{y0} and c_{z0}, one writes the magnetic field in sensor coordinates as

$$\begin{aligned} B_x &= k_x(c_x - c_{x0}), \\ B_y &= \alpha k_x(c_x - c_{x0}) + k_y(c_y - c_{y0}), \\ B_z &= \beta k_x(c_x - c_{x0}) + \gamma k_y(c_y - c_{y0}) + k_z(c_z - c_{z0}), \end{aligned} \tag{1}$$

where k_x, k_y and k_z are the scale factors for each axis and α, β and γ measure the contributions of X to the Y axis (α), X to the Z axis (β), and Y to the Z axis (γ), respectively, as off-diagonal elements of an alignment correction matrix (M)

$$[M] = \begin{bmatrix} 1 & 0 & 0 \\ \alpha & 1 & 0 \\ \beta & \gamma & 1 \end{bmatrix}. \tag{2}$$

In this case we have chosen the X-axis as the reference axis against which all misalignments are measured. Because the applied external field, B_{appl}, is the same for all orientations of the

sensor one can pose a least squares minimization problem defined by

$$\Delta^2 = \frac{1}{N}\sum_i \left(B_{x,i}^2 + B_{y,i}^2 + B_{z,i}^2\right) - {B_{\text{appl}}}^2, \tag{3}$$

where Δ is the residual to be minimized. Ideally one can also obtain an estimate of the zero-field offsets corresponding to each axis, c_{iO}, but convergence of the least squares solution is obtained much more rapidly if these offsets are determined independently such as from measurements in a magnetic shield or from "flipping" the sensor 180° in a weak ambient field. The low-range scale factors were determined by measuring the ratio of the responses in the high range to the low range in the laboratory once the high-range parameters had been established as described. The overall accuracy of the solutions is estimated at better than 0.1%.

The absolute alignment of the triaxial sensor assembly with respect to reference spacecraft coordinates after boom deployment is determined by means of spacecraft rolls in a moderate ambient field. Clearly, perfect alignment would imply no modulation along the axis parallel to the S/C roll axis and once more a least squares problem can be posed that estimates the alignment corrections that need to implemented to achieve this result.

6.2 Frequency Response and Timing

The overall frequency response of the magnetometer is determined by several contributors along the signal path, from the analog electronics to the digital output of the A/D converter. The first contributor is the intrinsic closed loop frequency response of the negative feedback system described in Sect. 4.1 for each axis. Typically the magnetometer is designed to have an intrinsic 3 dB cutoff frequency well above the desired signal roll-off characteristics and in the STEREO case the typical value is >60 Hz. A first-order output low-pass filter is then added at the output with a 16 Hz cutoff frequency to limit the analog bandpass and aliasing power present at the analog-to-digital converter input. This intrinsic frequency response is axis and range-dependent but the output low-pass filter normalizes the output bandwidth to a nominal range of 0 to 16 Hz within acceptable error limits. The typically steep f^{-n} characteristics of IMF fluctuations imply that the aliasing power contributed outside of the Nyquist frequency is small and a first-order low-pass filter is sufficient to ensure a reasonable and minimally aliased overall response. In addition, a first-order low-pass filter has minimal phase shift and the magnetometer amplitude and phase response can be easily inverted for spectral studies of the fluctuations of the IMF.

The sigma-delta A/D converter decimation output filter contributes additional amplitude and phase delays that can be represented as a Gaussian filter response or approximately constant time delay (∼6 ms). For additional details please refer to the CS5507 specification data sheet. All of these characteristics must be taken into account when spectral studies of the interplanetary magnetic field fluctuations at the highest time resolution of the magnetometer are carried out or when time correlations with other STEREO instrument data are desired.

6.3 Environmental Testing

The sensor assembly and electronics were environmentally tested at GSFC prior to spacecraft integration. Since high voltages and vacuum-sensitive components are not present in the magnetometer, initial thermal qualification testing was carried out in ambient air to reduce costs. Electrical performance as a function of temperature was tested over the range of

$-25°C < T < +65°C$; thermal cycling and survival tests were carried out over a temperature range 20°C wider at each extreme. Instrument performance was monitored exercising the analog step-calibration feature calibration and the A/D self-calibration capability. Determination of zero drifts with temperature is a time-consuming and difficult task because of the time variability of the typical laboratory magnetic environment (including that inside of multilayer magnetic shields) and historic in-flight performance must be used against comparative laboratory test data to estimate ultimate performance. For example, the Voyager magnetic field instruments (Behannon et al. 1977) provided almost 30 years of historical performance for this type of magnetic field instrument and show that under nominal conditions zero drifts are <0.2 nT/year. Thermal vacuum and final vibration testing were performed at the integrated IMPACT IDPU level at the Space Sciences Laboratory of the University of California Berkeley.

7 Spacecraft Magnetics Control Program

The success of weak interplanetary magnetic field measurements is intimately tied to the ability of the development team to control the magnetic fields generated by the spacecraft itself at the location of the MAG sensor (see Acuña 2002). Scientific measurements contaminated by spacecraft fields lead to controversy and inefficient use of limited resources in attempts to "clean up" the data. The STEREO project implemented a goal-oriented magnetics control program based on close cooperation among the experimenters and spacecraft builders. The objectives were to reduce as much as possible the static and dynamic fields generated by the spacecraft and experiments that introduce errors in the magnetic field measurements. For the static contribution, all components of the spacecraft employing magnetic materials (motors, actuators, relays, valves, RF isolators, etc.) were screened for magnetic signatures and compensation or reduction solutions developed where appropriate. The large contributions associated with the propulsion system valves and the communication system traveling wave tube amplifiers (TWTA) were canceled by adding permanent magnets mounted on the S/C bus. The dynamic (time variable) contribution is the most important since it is largely associated with variable currents circulating in the spacecraft, and its impact on the measurements cannot be easily eliminated by subtraction, spacecraft maneuvers, or modeling. Hence a set of "best engineering" practices must be followed to reduce their effect. For example, current loops associated with the power subsystem (battery, solar array, thermal control, power distribution system and spacecraft harnesses) were minimized using balanced twisted pairs for each major load and motors and actuators associated with the SECCHI instrument were magnetically shielded. The solar array layout and wiring was analytically optimized to reduce the associated magnetic field to a minimum while maintaining desirable electrostatic characteristics. Where "heritage" systems are involved and redesign or modification are not possible, artificial cancellation loops were used within the power distribution electronics as well and the battery cells were wired in a figure eight pattern and the orientations of the cells optimized to minimize the total magnetic moment of the battery.

To verify the success of the magnetics control program two system-level tests were conducted once the spacecraft were fully integrated: (a) a static magnetic moment assessment by measuring the dependence with distance of the spacecraft generated magnetic field, and (b) a magnetic compatibility test where all spacecraft subsystems are energized in a controlled sequence and the resulting magnetic field monitored with external test magnetometers.

8 Flight Checkout and Performance

The STEREO spacecraft were launched on October 25, 2006, and seven days later the IMPACT booms were deployed following the MAG activation. Figure 10 illustrates the magnetic field data acquired during the deployment of the "B" spacecraft boom. The data are not converted to physical units but are shown in counts to illustrate the automatic range control function. Prior to boom deployment the magnetometer sensor is close to the spacecraft bus and the highly magnetic TWTA and hence is in the HIGH range registering an elevated magnetic field value. When the boom deploys the measured field decreases rapidly to the lower digital threshold where the IDPU range control algorithm causes the magnetometer to switch to the low range increasing the sensivity of the instrument. The behavior of the measured field after the range change is dictated by the sequence of boom segment deployments with respect to the sensor position.

To estimate the effective values of the IMPACT/MAG zero offsets, a number of spacecraft roll maneuvers have been executed under a variety of ambient field conditions. Higher

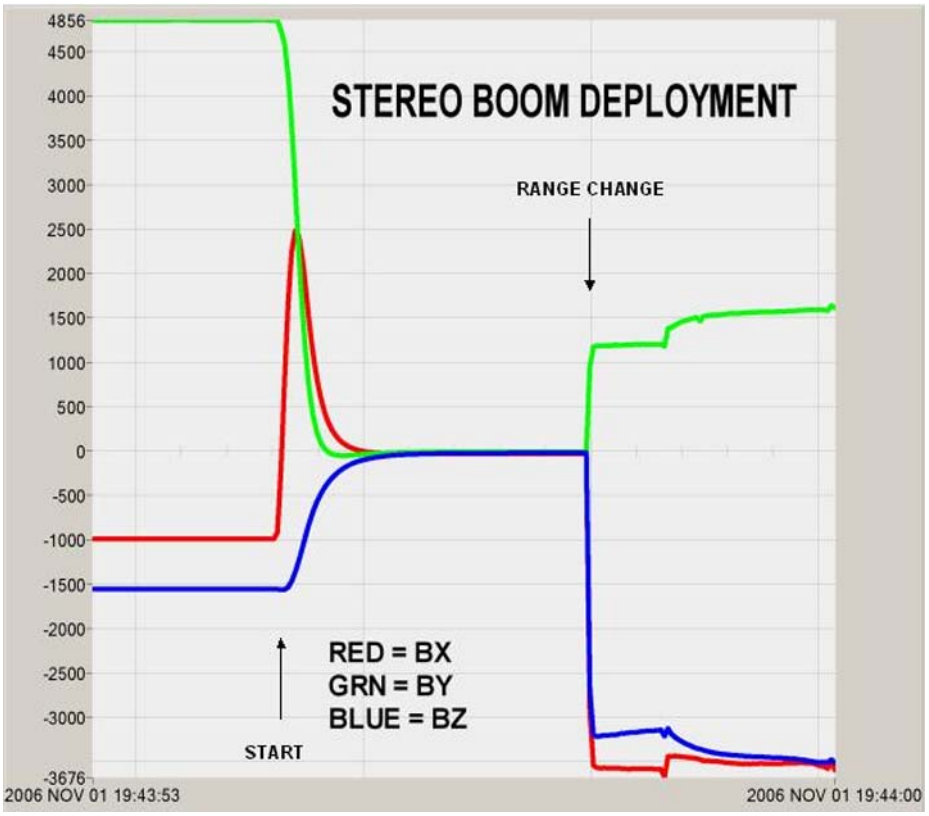

Fig. 10 MAG data acquired during the "B" spacecraft boom deployment. The data are shown in raw digital counts (±32,768) versus time. The magnetometer is initially in the HIGH field status (±65,536 nT) reading a relatively strong field associated primarily with the proximity to the TWTA magnets. As the boom deploys the readings decrease rapidly to zero until the automatic range change algorithm drives the magnetometer to the LOW range (±512 nT) causing the digital readings to increase. As the boom settles slowly into its fully deployed position the readings approach the sum of the ambient magnetic field plus spacecraft induced offsets

than expected zero offset values have been noted on both spacecraft and are attributed to the accidental magnetization of structural fasteners used to attach the MAG tray to the boom. Fortunately, these offsets can be successfully removed by spacecraft maneuvers and analytical techniques that take advantage of the statistical properties of the IMF (Acuña 2002; Schwarzl and Russell 2007). The analysis of the roll data also follows in general the strategy described by Acuña (2002). Since the spacecraft motion is known and the ambient field is approximately constant for very short periods of time, a least squares minimization problem can be posed as follows. The scalar product of the measured field (including offsets) times the change in the field due to the spacecraft motion can be written as a two-dimensional vector expression,

$$\mathbf{B}_{\mathrm{m}} \cdot \boldsymbol{\Delta}\mathbf{B} = (\mathbf{B}_{\mathrm{e}} \cdot \boldsymbol{\Delta}\mathbf{B}) + (\mathbf{Z} \cdot \boldsymbol{\Delta}\mathbf{B}), \tag{4}$$

where $\mathbf{B}_{\mathrm{m}}$ is the measured field, $\boldsymbol{\Delta}\mathbf{B}$ the instantaneous change in field due to rotation, $\mathbf{B}_{\mathrm{e}}$ the external field in the plane of the roll and $\mathbf{Z}$ is the unknown offset vector. It is clear that if the amplitude of the field does not change instantaneously between samples $\mathbf{B}_{\mathrm{e}} \cdot \boldsymbol{\Delta}\mathbf{B}=0$ and if we select a time series of sequential, two-dimensional vectors (bold) during the time that the spacecraft is rolling,

$$(\mathbf{B}_{\mathrm{m}})_i \cdot (\boldsymbol{\Delta}\mathbf{B})_i = \mathbf{Z} \cdot (\boldsymbol{\Delta}\mathbf{B})_{\mathrm{i}} \quad \text{for } i = 1, 2, 3, \ldots, n \text{ vectors} \tag{5}$$

we can obtain an estimate for $\mathbf{Z}$ as a solution to the least squares problem,

$$\mathbf{Z} = \left((\mathbf{B}_{\mathrm{m}})_i \cdot (\boldsymbol{\Delta}\mathbf{B})_{\mathrm{i}}\right)\left((\boldsymbol{\Delta}\mathbf{B})_i\right)^{-1}, \tag{6}$$

where $((\boldsymbol{\Delta}\mathbf{B})_i)^{-1}$ denotes the pseudo-inverse of the $((\boldsymbol{\Delta}\mathbf{B})_i)$ matrix.

This technique is particularly useful in cases where the ambient field is changing "adiabatically" (i.e., the field amplitude varies slowly with time without significant changes in direction) during a spacecraft roll as shown in Fig. 11 for the roll executed by spacecraft B on day 333 of 2006. The vertical and horizontal lines through the center of the spiral illustrate the solution obtained by the method described earlier. Significant advantages are the fact that sampling time information is not necessary and the ambient field need not be constant. The only knowledge required is that the spacecraft is rolling and the field is changing adiabatically. Note also that if we assume that all IMF fluctuations are changes in direction rather than amplitude, the technique described earlier can be used to estimate zero levels along all three magnetometer axes if the distribution of fluctuations is nearly isotropic during the interval of time considered (Acuña 2002; Schwarzl and Russell 2007).

9 Magnetometer Ground Data Processing

Magnetometer raw data records are produced at the University of California, Berkeley (UCB) and stored as Common Data Format (CDF) files. These data are sampled continuously at 8 Hz with occasional burst mode data (see Luhmann et al. 2007) obtained at 32 Hz. The data are then transferred to UCLA where one-second averages are produced of the raw data for use in the offset determination program (Schwarzl and Russell 2007). When offsets are changing slowly, less than about 0.3 nT/day the program can follow these changes to usually better than 0.1 nT. After the offsets are determined, Level-1 magnetometer records are made with all known corrections applied. The 8-Hz data (125 ms) are then averaged to one second resolution using overlapped averages of two seconds in length, and one-minute

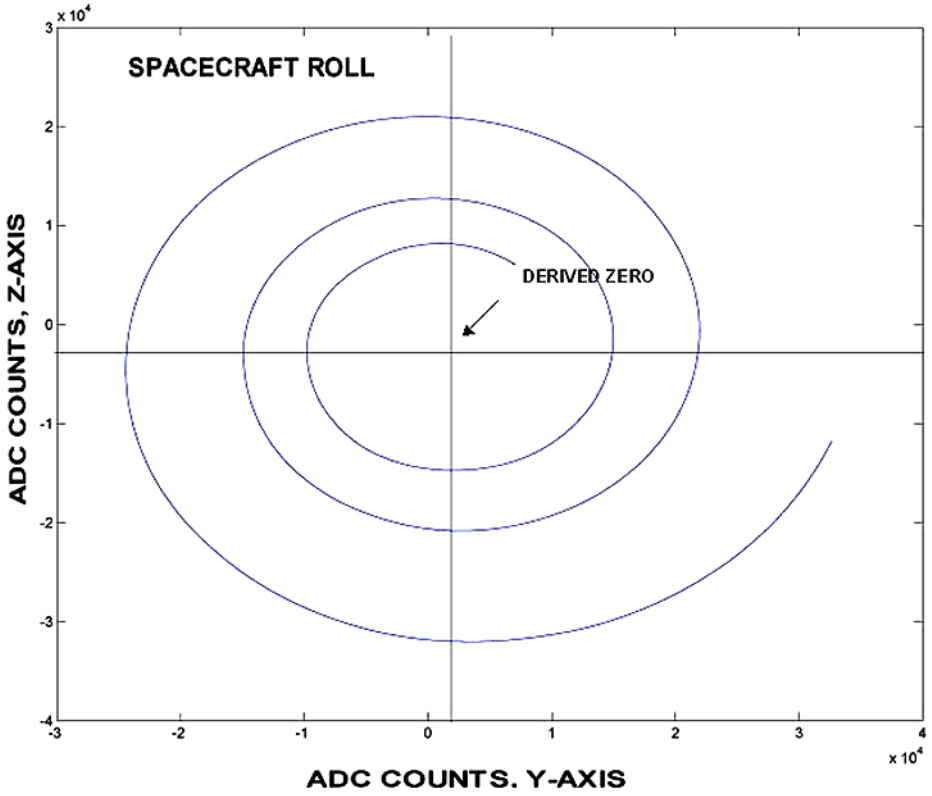

Fig. 11 A plot of Y-axis vs Z-axis digital readings during a spacecraft roll maneuver. A slowly varying ambient results in the spiral shown in the figure. The intersection of the *horizontal* and *vertical lines* illustrate the solution obtained by the method described in the text for estimating the zero level offsets in the roll plane

resolution data prepared with overlapped two-minute averages. These data are returned to UCB where CDF files are prepared. At UCLA the three data products (125 ms, 1 s, and 1 min) are rotated to RTN coordinates and stored in a Web-based data server with the original spacecraft coordinate data. Those using the data in geophysical studies will principally use the RTN system. Those using the magnetometer to reduce particle data will principally use the data in the spacecraft frame. The RTN (radial, tangential north) is defined so that R is radially outward with its origin at the Sun. The RN plane contains the rotation axis of the Sun and the T axis is in the direction of the cross product of the solar rotation axis and the Sun–spacecraft vector which is roughly in the direction of planetary motion. The spacecraft coordinates have X toward the Sun along the optical axis of the spacecraft. The Y and Z orientations about that direction are chosen to optimize communication with the Earth. Offset corrections are also made available, for use with UCLA-provided coordinate transformation software, to process STEREO beacon magnetometer data at the STEREO Science Center.

The processed magnetometer data are available both through the main IMPACT investigation data servers (see Luhmann et al. 2007) and the STEREO data archive at Goddard Space Flight Center. The near-real-time beacon data stream is available through the STEREO Science Center (see Thompson et al. 2007) and is also part of the archive. A descriptive example of fully processed data products is shown in Fig. 12 where we have plotted one-second averages of MAG data from both spacecraft in RTN coordinates for a period of

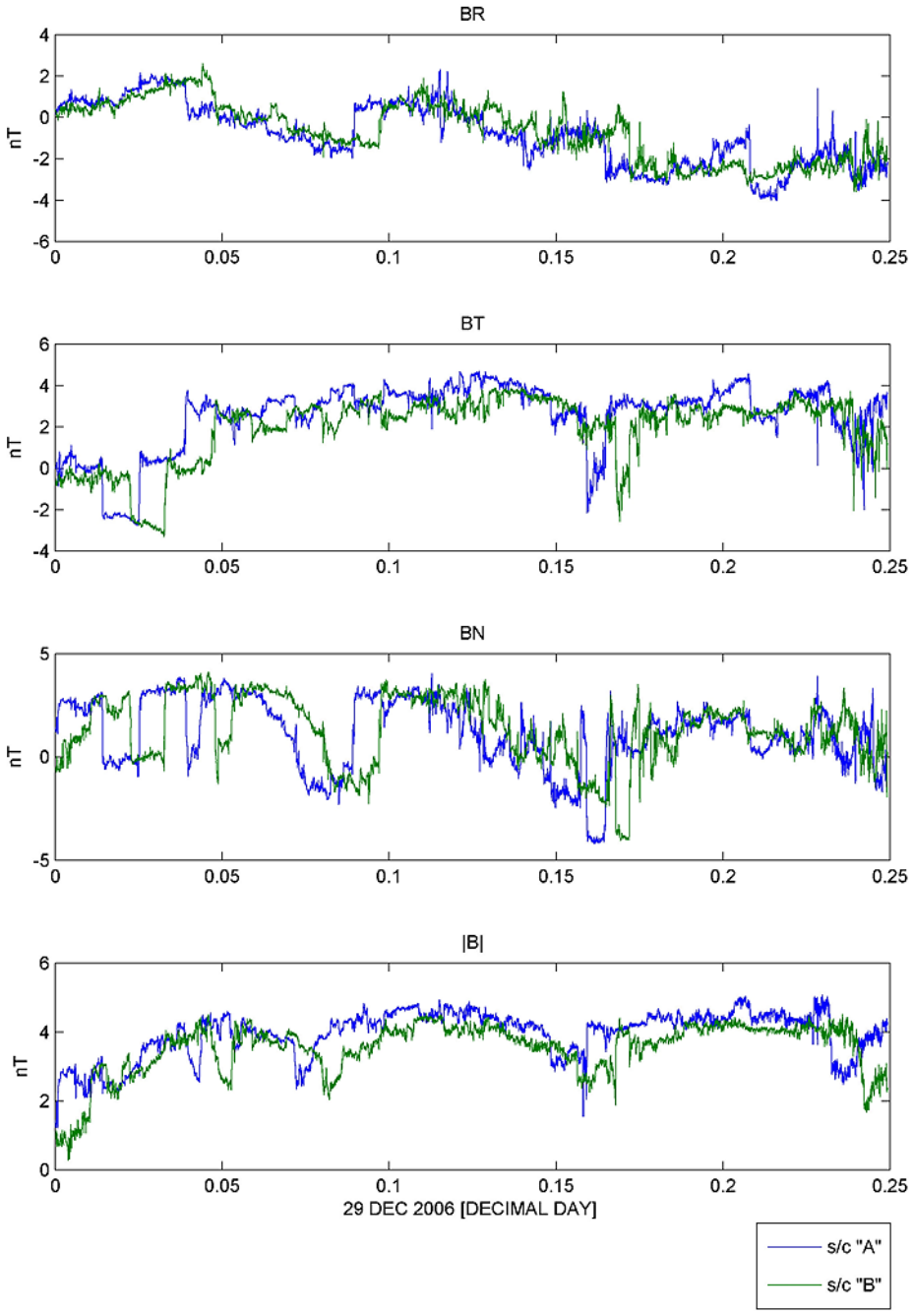

Fig. 12 A plot of IMPACT/MAG fully processed flight data from spacecraft "A" (*blue lines*) and spacecraft "B" (*green lines*) for a period of six hours on December 29, 2006. The *top three panels* correspond to the BR, BT and BN components while the bottom panel illustrates the magnitude of the field. Note that the IMF structures (mostly discontinuities) observed in spacecraft "A" lead in time the corresponding ones observed by spacecraft "B" as expected from the position of the spacecraft and co-rotation

six hours on December 29, 2006. Note that IMF structures are observed first by the "A" or ahead spacecraft and later by the "B" or behind spacecraft. This reflects both the radial position of the STEREO spacecraft as well as the effects of solar rotation on these structures.

Acknowledgements The authors thank the STEREO Project and the numerous individuals at Goddard Space Flight Center and JHU Applied Physics Laboratory who helped to ensure the quality of the STEREO magnetometer measurements. This work was supported as a Center-led portion of the STEREO IMPACT investigation.

References

M.H. Acuña, IEEE Trans. Magnetics **MAG-10**, 519 (1974)
M.H. Acuña et al., J. Geophys. Res. **97**(E5), 7799–7814 (1992)
M.H. Acuña, C.T. Russell, L.J. Zanetti, B.J. Anderson, J. Geophys. Res. **102**(E10), 23,751–23,760 (1997)
M.H. Acuña, Space-based magnetometers. Rev. Sci. Instrum. **73**(11), 3717–3736 (2002)
S.D. Bale, M.J. Reiner, J.-L. Bougeret, M.L. Kaiser, S. Krucker, D.E. Larson, R.P. Lin, Geophys. Res. Lett. **26**, 1573–1576 (1999)
K. Bamert, R. Kallenbach, N.F. Ness, C.W. Smith, T. Terasawa, M. Hilchenbach, R.F. Wimmer-Schweingruber, B. Klecker, Astrophys. J. **601**, L99–L102 (2004)
K.W. Behannon, M.H. Acuña, L.F. Burlaga, R.P. Lepping, N.F. Ness, F.M. Neubauer, Space Sci. Rev. **21**, 235–257 (1977)
L.F. Burlaga, *Interplanetary Magnetohydrodynamics* (Oxford University Press, New York, 1995)
L.F. Burlaga, R.P. Lepping, J.A. Jones, in *Physics of Magnetic Flux Ropes*, ed. by C.T. Russell, E.R. Priest, L.C. Lee. Geophys. Monogr. Ser., vol. 58 (AGU, Washington, 1990), pp. 373–378.
L.F. Burlaga, R.M. Skoug, C.W. Smith, D.F. Webb, T.H. Zurbuchen, A. Reinard, J. Geophys. Res. **106**, 20,957–20,978 (2001)
H.V. Cane, J. Geophys. Res. **93**, 1 (1988)
B.E. Gordon, M.A. Lee, E. Mobius, K.J. Trattner, J. Geophys. Res. **104**, 28,263–28,277 (1999)
J.T. Gosling, in *Physics of Magnetic Flux Ropes*, ed. by C.T. Russell, E.R. Priest, L.C. Lee. Geophys. Monogr. Ser., vol. 58 (AGU, Washington, 1990), pp. 343–364.
J.C. Kasper, W.C. Manchester IV, Astrophys. J. (2007, in press)
S. Koutchmy et al., Astron. Astrophys. **420**, 709 (2004)
D.E. Larson, R.P. Lin, J.M. McTiernan, J.P. McFadden, R.E. Ergun, M. McCarthy, H. Reme, T.R. Sanderson, M. Kaiser, R.P. Lepping, J. Mazur, Geophys. Res. Lett. **24**, 1911–1914 (1997)
M.A. Lee, J. Geophys. Res. **88**, 6109–6119 (1983)
R.P. Lepping, D.B. Berdichevsky, C.-C. Wu, A. Szabo, T. Narock, F. Mariani, A.J. Lazarus, A.J. Quivers, Ann. Geophysicae **24**, 215–245 (2006)
G. Li, Q. Hu, G.P. Zank, in *The Physics of Collisionless Shocks*, ed. by G. Li, G.P. Zank, C.T. Russell. AIP Conference Proceedings, vol. 781 (Melville, New York, 2005), pp. 233–239
D.A. Lohr, L.J. Zanetti, B.J. Anderson, T.A. Potemra, J.R. Hayes, R.E. Gold, R.M. Henshaw, F.F. Mobley, D.B. Holland, M.H. Acuña, J.L. Scheifele, Space Sci. Rev. **82**(1,2), 255–281 (1997)
J.G. Luhmann et al., Space Sci. Rev. (2007, this issue). doi:10.1007/s11214-007-9170-x
J.M.G. Merayo, P. Brauer, F. Primdahl, J.R. Petersen, O.V. Nielsen, Meas. Sci. Tech. **11**, 120–132 (2000)
R.A. Mewaldt, C.M.S. Cohen, A.W. Labrador, R.A. Leske, G.M. Mason, M.I. Desai, M.D. Looper, J.E. Mazur, R.S. Selesnick, D.K. Haggerty, J. Geophys. Res. **110**, A09–S18 (2005). doi:10.1029/2005JA011038
T. Mulligan, C.T. Russell, J. Geophys. Res. **10**, 581 (1999)
T. Mulligan, C.T. Russell, B.J. Anderson, D.A. Lohr, D. Rust, B.A. Toth, L.J. Zanetti, M.H. Acuña, R.P. Lepping, J.T. Gosling, J. Geophys. Res. **104**, 28,217 (1999)
F.M. Neubauer, M.H. Acuña, L.F. Burlaga, B. Franke, B. Gramkow, J. Phys. E **20**, 714–720 (1987). ISSN 0022-3735
M. Neugebauer, R. Goldstein, in *Coronal Mass Ejections*, ed. by N. Crooker, J. Joselyn, J. Feynman. AGU Geophys. Mon., vol. 99 (Washington, 1997), p. 245
D. Odstrcil, P.C. Riley, X.P. Zhao, J. Geophys. Res. **109** (2004). doi:10.1029/2003JA010135
G. Paschmann, N. Sckopke, S.J. Bame, J.T. Gosling, Geophys. Res. Lett. **9**, 881–884 (1982)
T.A. Potemra, L.J. Zanetti, M.H. Acuña, IEEE Trans. Geosci. Remote Sens. **GE-23**, 246 (1985)
I.G. Richardson, H.V. Cane, J. Geophys. Res. **98**, 15,295–15,304 (1993)
I.G. Richardson, H.V. Cane, Geophys. Res. Lett. **31**, L18804 (2004). doi:10.1029/2004GL020958

J.D. Richardson, K.I. Paularena, Geophys. Res. Lett. **25**, 2097 (1998)
D.A. Roberts, M.L. Goldstein, L.W. Klein, W.H. Matthaeus, J. Geophys. Res. **92**, 12,023–12,035 (1987)
D.A. Roberts, M.L. Goldstein, W.H. Matthaeus, S. Ghosh, J. Geophys. Res. **97**, 17,115–17,130 (1992)
C.T. Russell, J.T. Gosling, R.D. Zwickl, E.J. Smith, J. Geophys. Res. **88**, 9941 (1983)
T.R. Sanderson, R. Reinhard, P. van Nes, K.P. Wenzel, J. Geophys. Res. **90**, 19–27 (1985)
H. Schwarzl, C.T. Russell, J. Geophys. Res. (2007, to be submitted)
O.C. St.Cyr, J.M. Davila, in *Space Weather*, ed. by P. Song, H.J. Singer, G.L. Siscoe. AGU Geophys. Mon., vol. 125 (Washington, 2001), pp. 205–209
A. Szabo, J. Geophys. Res. **99**, 14,737–14-746 (1994)
A. Szabo, D.E. Larson, R.P. Lepping, in *Proceedings of Solar Wind Nine*, ed. by S.R. Habbal, R. Esser, J.V. Hollweg, P.A. Isenberg (AIP, Woodbery, 1999), pp. 589–592
A. Szabo, R.P. Lepping, J. Merka, C.W. Smith, R.M. Skoug, in *Proceedings of "Solar Encounter: The First Solar Orbiter Workshop"*, ed. by E. Marsch, V. Martinez Pillet, B. Fleck, R. Marsden. ESA, vol. SP-493 (Puerto de la Cruz, Tenerife, Spain, 2001), pp. 383–387
A. Szabo, in *The Physics of Collisionless Shocks*, ed. by G. Li, G.P. Zank, C.T. Russell. AIP CP, vol. 781 (Melville, New York, 2005)
Thompson et al., Space Sci. Rev. (1985, this issue). doi:10.1007/s11214-007-9249-4
A.F. Viñas, J.D. Scudder, J. Geophys. Res. **91**, 39–58 (1985)
L.J. Zanetti, T.A. Potemra, R.E. Erlandson, P. Bythrow, B.J. Anderson, A.T.Y. Lui, S. Ohtani, G. Fountain, R. Henshaw, B. Ballard, D. Lohr, J. Hayes, D. Holland, M.H. Acuña, D. Farifield, J. Slavin, W. Baumjohann, M. Engebretson, K.-H. Glassmeier, T. Iijima, H. Luehr, F. Primdahl, Space Sci. Rev. **70**, 465–482 (1994)
G.P. Zank, G. Li, G.M. Webb, J.A. Le Roux, V. Florinski, X. Ao, W.K.M. Rice, in *The Physics of Collisionless Shocks*, ed. by G. Li, G.P. Zank, C.T. Russell. AIP Conference Proceedings, vol. 781 (Melville, New York, 2005), pp. 170–179
R.D. Zwickl, J.R. Asbridge, S.J. Bame, W.C. Feldman, J.T. Gosling, E.J. Smith, in *Solar Wind Five*, ed. by M. Neugebauer. NASA Conference Publication, vol. 2280 (JPL, 1983), pp. 711–718